110th Anniversary: Syngas Production Enhancement Using Calcium- and Potassium-Impregnated Chars

Marion Ducousso,*[,†] Elsa Weiss-Hortala,[†] Nathalie Lyczko,[†] Ange Nzihou,[†] and Marco J. Castaldi[‡]

[†]RAPSODEE, CNRS UMR 5203, Mines Albi, Campus Jarlard, 81013 Albi, CT Cédex 09, France

[‡]Chemical Engineering Department, The City College of New York, City University of New York, Convent Ave. at 140th Street, New York, New York 10031, United States

ABSTRACT: Syngas production enhancement via catalytic methane cracking onto metal-loaded chars, with a specific focus on the activity of two inherent alkali and alkaline earth metals (AAEMs), Ca and K, was investigated. Chars produced from the gasification of poplar wood pellets were heated to 700 °C in an inert atmosphere and then tested as catalysts for methane cracking at 700 °C. Methane is one of the most abundant biomass gasification byproducts. The cracking of this component is relevant in increasing the syngas production and yield. The syngas production was increased by a factor 1.9−2.7 using metal-loaded chars. Results were explained by the catalytic effect of AAEMs on both the desorption of oxygenated functional groups and on the catalytic methane cracking. AAEMs promoted methane molecule combination with the active sites such as oxygenated groups available at the surface of the chars enhancing both H_2 and CO production. It was observed that potassium-loaded char (K-char) showed the best performance. The calcium-loaded char (Ca-char) was less efficient, due to a higher amount of silicon that interacted with calcium to form silicates. No synergetic effect was observed on the syngas production with the Ca+K-char.

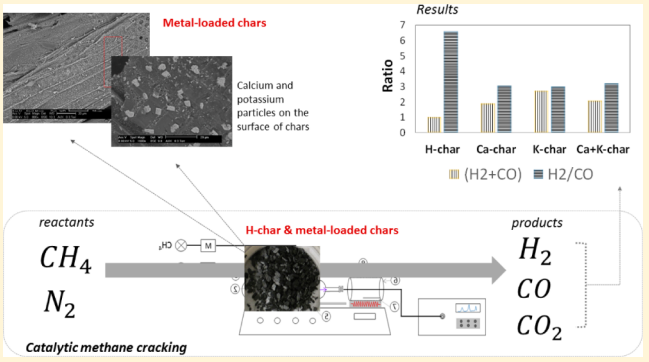

1. INTRODUCTION

Currently, char utilization is gaining momentum. It has been recently explored as an renewable resource, potentially less expensive than activated carbon. Physico-chemical and thermal properties of the char are notable and motivate its utilization for various applications such as adsorption for wastewater and air pollution treatments,[1−5] soil amendment,[6−8] supercapacitance,[9] and catalysis.[10−12] Comprehensive reviews were published in the past few years that emphasize the worldwide interest in the topic.[13−15] Among the different applications, the reintroduction of chars into the gasification process as catalyst for the cleaning and upgrading of the syngas in a carbon loop closing has been proposed.[16−18] Syngas, which is the most value-added product from the gasification process, could be valorized in different applications such as producing methanol, ammonia, or synthetic fuel through Fischer−Tropsch synthesis. Saad et al.[19] highlighted the importance of meeting a particular H_2/CO molar ratio according to the end-use product processing requirement: Fischer−Tropsch reaction (H_2/CO = 2), methanol synthesis (H_2/CO = 2), aldehyde and alcohol production (H_2/CO = 1). While Cao et al.[20] depicted the interest in a downstream facility to adjust the H_2/CO molar ratio and the growing interest in an alternative technology for cost-effective production of syngas. Hence, the use of the char as a catalyst for the syngas production enhancement and H_2/CO ratio adjustment is of particular interest since it represents an on-site valorization of the char and should positively influence the economics of gasification unit. In this study, the focus is on the catalytic methane cracking in a char fixed bed. Methane is the second most concentrated byproduct in the output gas of a gasifier[21] (after CO_2). Its cracking can significantly improve the yield of biomass conversion into syngas and it represents a possibility to adjust the H_2/CO ratio since the reaction produces additional hydrogen (see eq 1). Parallel reactions with oxygenated groups from the surface can produce carbon monoxide as well.[22,23]

$$CH_{4(g)} \rightarrow 2H_{2(g)} + C_{(s)} \quad (1)$$

Char is usually described as a porous carbonaceous material with a specific surface area up to 1000 m^2/g (depending on the biomass and the thermal treatment).[15] Chars coming from woody biomass conversion are mostly composed of carbon atoms (about 80 wt $\%_{daf}$, ECN Phyllis Classification), forming short-range ordered structures in which various heteroatoms such as oxygen, hydrogen, and nitrogen and inorganic components like alkali and alkaline earth metals (AAEMs) or silicates and sulfur can be incorporated.[17] From a catalytic standpoint, this inherent inclusion and dispersion of AAEMs

particles onto the porous carbonaceous surface is an advantage. Most commercial catalysts are composed of a porous substrate (generally nonreactive) on which metal particles are dispersed.[24] This similarity of surface properties between chars and metal supported catalysts connects the idea that inherent AAEMs of the chars could be involved in their reactivity. Therefore, the understanding of the role of the AAEMs particles incorporated into the chars on catalytic reactions could broaden application fields.

Carbonaceous catalysts, such as activated carbon, carbon black, or more ordered carbons, have already been investigated for methane cracking. The outcome of those studies reveals that the reaction mechanism is complex and it is dependent on both the chemistry and the textural properties (i.e., specific surface area and porosity) of the carbon.[25−27] Some studies investigated the role of the intrinsic metals contained in the carbon catalyst.[28,29] Klinghoffer et al.[28] removed the ash content of chars (via acid washing treatment) prior to a methane cracking test and compared the catalytic activity with the H-char. It was concluded that the activity was enhanced in the presence of inherent metals by 18%. It has also been highlighted that the interaction between the carbon matrix and the inherent metal particles of the char was a key parameter since the ash, taken alone, was less efficient than the H-char. Feng et al.[29] investigated the re-forming of model tar compounds on Ca- and K-loaded chars using either a steam or CO_2 atmosphere. They found that the cracking reaction was enhanced on AAEMs loaded chars due to the increase of functional groups and defects on the char. However, they did not study the final gas product composition. These results are aligned with studies demonstrating that the gasification is catalyzed by the AAEMs inherent to the biomass.[30−34] Notably, potassium has a catalytic effect on the reaction.[35−37] Significant insights in the mechanisms occurring during gasification were provided: the potassium particles behave as a bridge between the reactant gas (CO_2, air or steam vapor) and the carbon atoms in the surface of chars and play a key role.[32] A similar effect likely occurs with calcium and sodium, but they are less reactive for gasification reaction.[38] The influence of AAEMs on the methane cracking reaction onto chars has been less studied so far. It is possible that the AAEMs play a similar role by transferring hydrogen atoms from the methane molecule to the carbonaceous surface of the chars. Hence, AAEMs could represent active sites during methane cracking reaction onto chars. Being able to quantify their catalyst efficiency is a key point in the potential use of catalysts produced from chars for methane cracking reaction.

This study focuses on the possibility of increasing the syngas yield and its quality using metal-loaded chars as a catalyst for the methane cracking reaction. Metal impregnation was performed on wood prior to the gasification step. Chars impregnated with calcium and potassium were tested for the reaction at 700 °C and characterized. The influence of the chars on the efficiency of the syngas production and the molar H_2/CO ratio was investigated and discussed in correlation with the physicochemical properties of the chars.

2. EXPERIMENTAL SECTION

This section describes the following experimental steps in the order they were performed; the raw poplar wood chips impregnation with nitrate salts solutions, the gasification process, the physicochemical characterizations of the surface of the chars, and the catalytic methane cracking tests.

2.1. AAEMs Impregnation of Poplar Wood Chips. Poplar wood chips (4 mm × 4 mm × 1 mm) were impregnated with nitrate salt solutions of either calcium ($Ca(NO_3)_2$), potassium (KNO_3), or both. The use of nitrate salts was selected since they decompose under heating. However, sulfate, phosphate, chloride, and carboxylate are more thermally stable and may not convert to the forms desired.[39] The same protocol was followed for the three impregnations. A solution of nitrate salt containing 1 wt % of the AAEM of interest (Ca, K and a mixture) was prepared. Thirty grams of poplar wood chips was immersed in 300 mL of solution during 6 h. Regarding the simultaneous impregnation of calcium and potassium, the solution prepared contained 0.5 wt % of calcium and potassium, respectively. The solution was stirred using a magnetic stirring rod throughout the process to allow sufficient mass transfer. The impregnated poplar wood chips were dried overnight at 105 °C following the NF-M03-002 protocol. Thus, three types of metal-impregnated poplar wood samples have been prepared and the corresponding chars after gasification are named: Ca-char, K-char, and Ca+K-char.

2.2. Gasification of Raw and Metal-Impregnated Poplar Wood Chips. Gasification of the raw and metal-impregnated poplar wood chips was performed following the same operating conditions. A 65 g amount of poplar wood chips (furnished by Lithaspen company) was gasified into a fluidized bed reactor (custom-made stainless steel) with an internal diameter of 6.1 cm and a height of 59.9 cm. This reactor was equipped with a frit on the bottom to hold the biomass, and 10 thermocouples were placed throughout the reactor in the vertical direction to measure the temperature profile. The temperature was controlled with a Eurotherm temperature controller that was connected to a thermocouple placed in the center (vertically and radially) of the reactor. Gasification experiments were performed at 750 °C during 30 min into a 90 vol % H_2O/10 vol % N_2 mixture (purity: 99.5%) atmosphere of 400 SPLM kg^{-1} of biomass (SPLM is standard liters per minute).

Prior to the gasification, the poplar wood was ground into chips of about 4 mm × 4 mm × 1 mm. Minimum fluidization tests were performed using a manometer with a liquid column (MVI 1500 type, liquid: tetrabromide) connected to two entrances at different heights of the fluidized bed. It has been experimentally found that from 260 SPLM kg^{-1} of biomass the bed of wood chips is fluidized. Post-testing, gasification chars have been crushed with a mortar and pestle and sieved to obtain particles with diameters between 100 and 125 μm.

2.3. Catalytic methane Cracking on Chars. Catalytic methane cracking tests were performed in a thermogravimetric analyzer (951 Dupont Instrument) coupled with a gas chromatograph (Agilent 3000A) to record simultaneously the gas production (H_2, CO, and CO_2) and the mass variation (see Figure 1). The 951 thermogravimetric analyzer from Dupont Instruments is a horizontal module composed of two separate chambers disposed on the two sides of the balance housing. The first chamber made of glass contains the counter weight arm, the lamp, and the photovoltaic cells (Figure 1, #2 and #3). This chamber is under an inert environment to prevent any oxidation of the system. The secondary chamber is made of quartz, it is 206 mm long with an internal diameter of 22 mm. It contains the quartz rod holding the platinum pan where the sample is deposited (Figure 1, #4). A thermocouple is positioned on the right side of the pan to record the temperature in close proximity to the sample (Figure 1, #5).

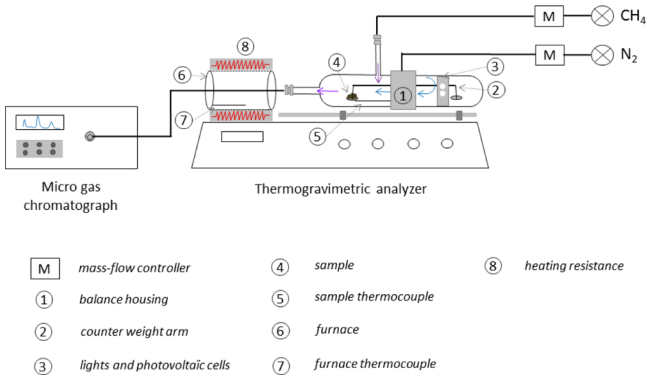

Figure 1. Illustration of the thermogravimetric analyzer coupled with a micro GC for the methane cracking experiments on the chars.

This quartz reactor is composed of two entrances: one dedicated to the nitrogen flow rate and a second one for the methane introduction. The entire module is designed to be translated to place the second chamber into the external 500 W furnace. A thermocouple located close to the furnace wall monitors furnace temperature heated by electric resistances (Figure 1, #7 and #8).

Twenty milligrams of crushed chars ($100 < d_p < 125$ μm) was introduced into the reactor. The sample was first heated in pure nitrogen with a heating rate of 20 °C/min and held for 30 min at 700 °C to stabilize the temperature prior to the introduction of the methane mixture. Then, it was exposed to a mixture of 10 vol % CH_4/90 vol % N_2 with a flow rate of 80 mL/min (TYLAN mass flow controller). The gas phase effluent was analyzed online using a gas chromatograph (Agilent 3000A) with four channels enabling detection of permanent gases to C7 hydrocarbons and TCD detectors, which allow the detection of light gases and more specifically hydrogen. Preliminary tests using an empty crucible were performed, and no methane conversion into hydrogen was detected.

2.4. Characterization of Chars. *2.4.1. Ultimate Analysis and Ash Content Determination.* The measurements of the ash content were performed following the French standards NF-EN-14775 (AFNOR 2010).[40] The ultimate analysis was carried out on an elemental analyzer (CE instrument NA 2100). The determination of C, H, N, and S was made by using complete combustion in excess of air. CO_2, NO_2, and SO_2 have been separated by a gas chromatograph column and then quantified via a TCD detector.

2.4.2. Metal Content. Quantification of inorganics, including the calcium and potassium, was performed using an Energy Dispersive X-ray fluorescence spectrometer (EPSILON 3XL from PANanalytical company) equipped with a silver anode of 15 W electrical power. The resolution range of the Silicium Drift SDD detector was between 135 eV and 5.9 keV.

Characterization of the inorganics chemical state and structures was investigated by XRD analyses using a Philips diffractometer (from PANalytical, X'pert Pro MPD model) with a $\theta-\theta$ Bragg–Brentano configuration, a current of 45 kV, and an intensity of 40 mA. The X-ray tubing is copper, and its radiation wavelength is of 1.543 E. Diffraction peaks were recorded in the 10–70° in 2θ and a speed of 0.042°/s. The peak assignment was based on the JCPDS and COD databases.

The metal particles dispersion, morphology, and local composition were investigated by ESEM coupled with EDS (ESEM, FEI XL30).

2.4.3. Gas Adsorption Measurements. Gas adsorption measurements were carried out on an ASAP 2010 apparatus from Micromeritics. Adsorption of argon was monitored at 77 K until a relative pressure of 1 atm. Argon was chosen rather than nitrogen because its molecular overcrowding is lower than the one of nitrogen and is more adapted to characterize our sample. Prior to argon adsorption a degassing step of 30 h under high vacuum at 200 °C was performed. The specific surface area was determined by application of the Langmuir model. The total micropore volume and mean pore diameter were evaluated using the Horvath–Kawazoe model.

3. RESULTS AND DISCUSSION

3.1. Chars Characterization. The ultimate analysis, ash content, and concentrations of Ca, K, Mg, and Si of H-char and metal-loaded chars are provided in Table 1. The calcium and potassium contents are below 1 wt % (0.6 and 0.7 wt % respectively) in the H-char. The calcium content is 5.4 wt % in the Ca-char while the potassium content is 5.3 wt % in the K-char. The Ca+K-char has an equal composition in calcium and potassium (2.3 and 2.4 wt %). In Figure 2, one can observe

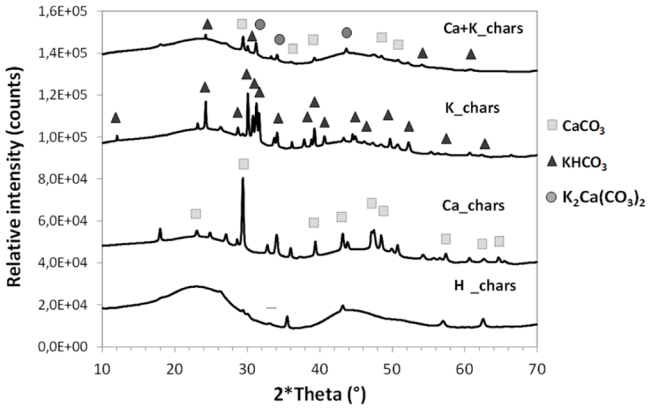

Figure 2. X-ray patterns of the H-char and metal-impregnated chars.

Table 1. Ultimate Analysis, Ash Content, and Main Inorganics Concentrations (Ca, K, Mg, Si; Determined by XRF) of the Chars (wt $\%_{dry,basis}$)

	C	H	N	O[a]	Ca	K	Mg	Si	ash
H-char	82.5	2.2	0.5	13.2	0.6	0.7	0.2	0.1	3.8
Ca-char	74.1	1.5	0.2	18.3	5.4	0.1	0.1	0.3	17.9
K-char	69.6	1.9	0.1	22.5	0.3	5.3	0.2	0.1	21.4
Ca+K-char	77.6	1.9	0.2	15.4	2.3	2.4	0.1	0.1	16.9

[a]Calculated [O] = 100 − [C] − [H] − [N] − [inorganics].

that Ca and K elements are present in carbonate crystalline forms ($CaCO_3$ and K_2CO_3) in the H-char. According to the operating conditions and the literature, carbonates of AAEMs were expected at the H-char surface.[41] In addition, ESEM analyses were performed to observe the local distribution of the metal particles at the H-char surface. The small fractions of inorganic species (less than 5 wt $\%_{dry\ basis}$) are heterogeneously distributed onto the char surfaces (see Figure 3).

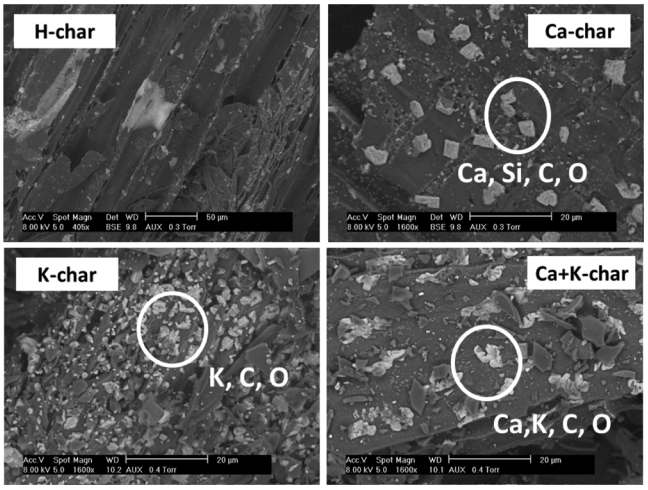

Figure 3. ESEM images of (A) H-char, (B) Ca-char, (C) K-char, and (D) Ca+K-char.

For the Ca-char, the concentration of calcium is 10 times higher than in the H-char. It is equal to 5.4 wt $\%_{dry\ basis}$. EDS microanalysis performed together with the ESEM characterization confirmed a homogeneous dispersion of the metal particles (1−5 μm) onto the chars. It also highlighted the presence of $CaCO_3$ crystals as hexagonal plates and complex inorganic forms in which both calcium and silicon were contained (see Figure 3). In fact, it is pointed out in the literature that calcium can be incorporated into silicon structures that are poorly soluble.[41−44] The higher amount of calcium particles at the Ca-char surface favored the formation of calcium silicates, which were more stable at the char surface during the gasification process ($T_{fusion,\ silicate} > T_{fusion,silicon}$). This confirms the ability of calcium to conjugate with silicon and to retain it at the surface of chars (0.3 wt % compared to 0.1 wt $\%_{dry\ basis}$ for the H-char).

Regarding the K-char, the potassium content was increased by a factor 8 and reached a value of 5.3 wt $\%_{dry\ basis}$. From a literature report,[45] it could be expected that the combined presence of K, steam, and CO_2 (mainly from wood gasification) could form either K_2CO_3 or $KHCO_3$. In the K-char, potassium was detected in the bicarbonate form (see Figure 2) and it is homogeneously distributed at the surface as micrometer dispersed particles (see Figure 3). No complexes with silicon or other inorganic species were detected at the surface of the chars by ESEM+EDS measurement. Concentrations of the alkaline earth metals (Ca, Mg) decreased by 56 and 21%, respectively, while the silicon content was comparable to the one of the H-char.

For the Ca+K-char, amounts of calcium and potassium are 4 times higher than their concentrations in the H-char (see Table 2). ESEM images of the surface show micrometer-scale metal particles, well dispersed at different locations of the surface (see Figure 2). EDS measurements revealed that, in addition to particles of potassium and calcium identified separately, complex structures containing both of these two species were present, which could be $K_2Ca(CO_3)_2$ as determined by other research groups (see Figure 3).[46]

Table 2. Langmuir Specific Surface Area and Total Volume of Micropores of the Chars Determined by Gas Adsorption

char	specific surface area (m^2/g)	total volume of micropores (cm^3/g)	mean pore diameter (μm)
H- char	662	0.22	5
Ca-char	619	0.24	5
K-char	446	0.15	10
Ca+K-char	346	0.11	10

Hence, it was confirmed that the concentration of the AAEMs of interest (Ca and K) efficiently increased in the three metal-loaded chars and a good dispersion of the AAEMs particles onto the surface of the chars was observed. The next section discusses the correlations between the added metals and the physical properties.

Gas adsorption measurement reveals that the H-char is a microporous material with a specific surface area of 662 m^2/g and a total micropore volume of 0.22 cm^3/g (Table 2). By impregnating the raw poplar wood before pyro-gasification, the resulting chars showed a decrease in the specific surface area to reach 619, 446, and 346 m^2/g for Ca-char, K-char, and Ca+K-char, respectively. Regarding the Ca-char, its specific surface area, total micropore volume and mean pore diameter are within the same order of magnitude compared to the H-char. For K-char and Ca+K-char, the impregnated wood does not develop the same specific surface area during pyro-gasification. The mean pore diameter is of 10 μm for these two chars.

3.2. Methane Cracking Tests. The tests were composed of two steps: initial heating from ambient to 700 °C in an inert gas (pure nitrogen) and then the isothermal methane cracking at 700 °C for 2 h. Gas production (notably H_2 and CO but also CO_2 during the heating) was evaluated for the four chars.

Figure 4 presents the CO_2 and CO productions over the heating to 700 °C prior to the introduction of the methane. One can observe that the three metal-impregnated chars present higher CO and CO_2 productions than the H-char. Various oxygenated functions (acidic, basic) are present at the surface of chars. During a thermal treatment, these functions could desorb from the surface and produce CO and CO_2 if they are not stable. Strong acid functions, desorbing from 200 to 600 °C, produce CO_2 while CO will be generated by the desorption of weak acidic and basic oxygenated functions (phenol and carbonyl) for a temperature above 600 °C. The stability of the oxygenated groups onto char surfaces has been studied in detail and reported in a previous paper.[46] Such an impact of AAEMs on the production of CO_2 and CO during thermal treatments of metal-loaded chars (of biomass or coal) has already been reported in the literature.[47−49] Feng et al.[29] highlighted that the presence of AAEMs increase the formation of oxygenated functions at the surface of the chars during gasification.

Reactions involving AAEMs species also occur during the heating. Focusing on the Ca-char behavior, the instantaneous CO_2 production is comparable to the H-char up to 600 °C. Then, significantly higher gas production is observed at 650−700 °C. The CO_2 production increase at 650 °C is likely due to the transformation of calcium carbonate into calcium oxide.

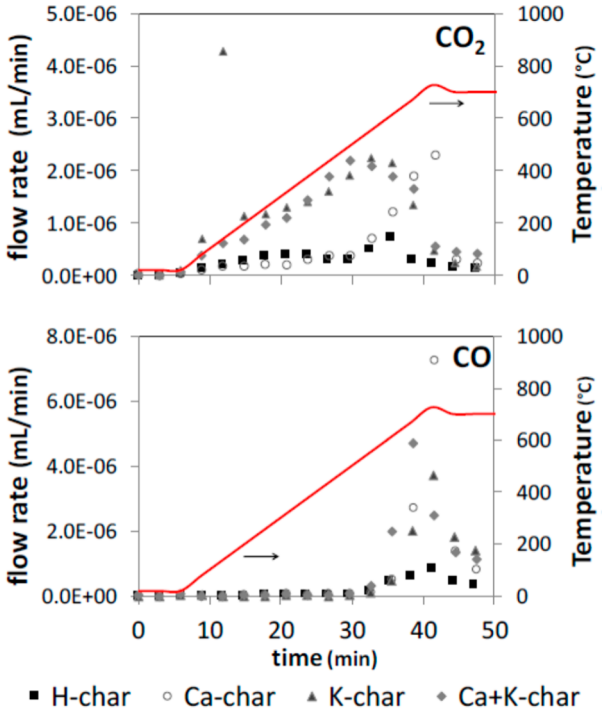

Figure 4. Gas production during heating to 700 °C in pure N_2 (72 mL/min (at 0 °C, 1 atm), 20 mg of char, 20 °C/min): (A) CO_2 and (B) CO.

In fact, Kannan et al.[50] reported that this reaction should normally occur at higher temperature (898 °C). However, due to interactions with the carbon matrix, the carbonate decomposition takes place at a much lower temperature. This is in agreement with previous works performed by McKee et al.[51] Regarding the K-char, a significant peak of CO_2 is observed at low temperature (200 °C). This corresponds to the transformation of $KHCO_3$ into K_2CO_3.[52] An estimation of the CO_2 production indicates that all the bicarbonates should have been transformed into carbonates.

Figure 5 shows the instantaneous gas production (H_2, CO) of the H-char and metal-loaded chars over the methane cracking reaction (700 °C). Hydrogen production and mass gain are higher for the metal-loaded chars than for the H-char char, which highlights the catalytic effect of the AAEMs particles on the methane cracking reaction (see eq 1). The K-char shows the best performances, enhancing by a factor 4 the initial hydrogen production while the Ca-char and the Ca+K-char show similar performances, increasing the initial hydrogen production by a factor 2. After 2 h, the hydrogen production of the H-char and metal-loaded chars decrease to a quasi-similar rate. This is due to the deactivation of the char surface.[53,54] In fact, Figure 6 shows the mass gain for the 4 chars, which confirms the carbon desposit via reaction eq 1. One can observe that the mass gain is in the following ascending order: H-char < Ca-char < Ca+K-char < K-char, which is consistent with the observed gas productions. During the isothermal methane cracking, CO and CO_2 were detected. Their production likely comes from the reaction of the methane molecules and the oxygen atoms, which remain (mostly basic functions[46]) at the char surface ($\sim O_{surf}$; see eqs 2 and 3). In fact, it has been highlighted in the literature that oxygenated functions that are stable at a temperature above 700 °C (i.e., carbonyl, pyrone) could be reactive sites for methane

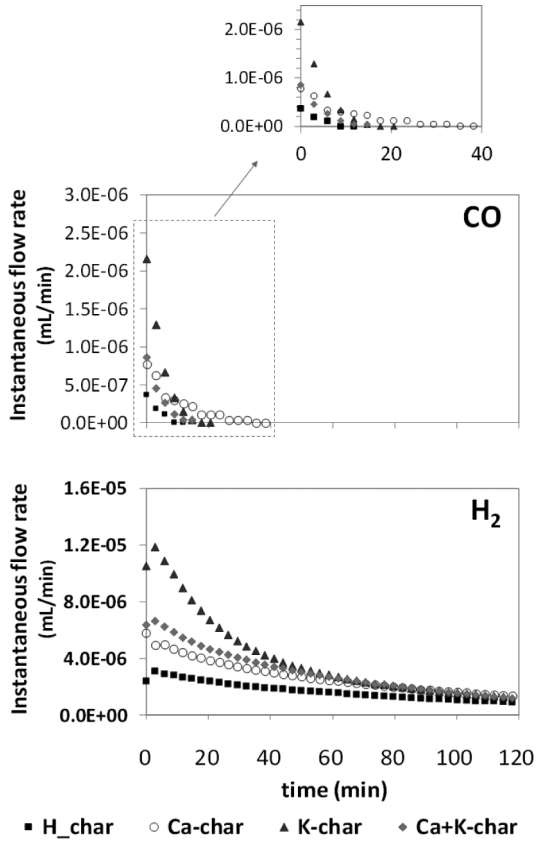

Figure 5. Instantaneous flow rate (H_2 and CO; mL/min) produced by the catalytic methane cracking experiment at 700 °C for 2 h on a fixed bed of 20 mg of chars in an atmosphere of 10 vol % CH_4/90 vol %N_2 at a total flow rate of 80 mL/min (at 0 °C, 1 atm).

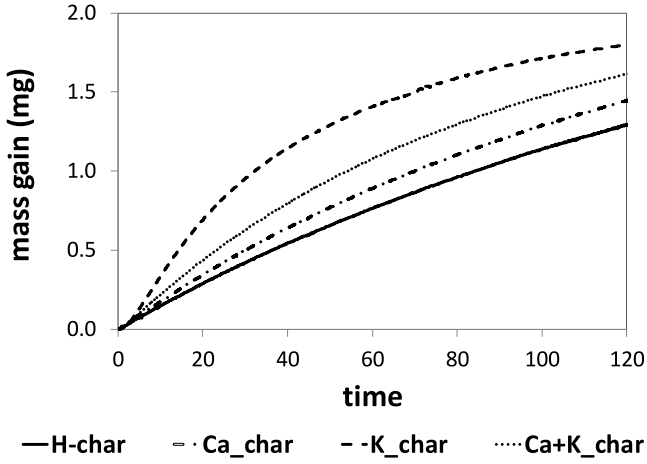

Figure 6. Mass gain during the catalytic methane cracking experiment at 700 °C for 2 h on a fixed bed of 20 mg of chars in an atmosphere of 10 vol % CH_4/90 vol % N_2 at a total flow rate of 80 mL/min (at 0 °C, 1 atm).

cracking.[27,55] As it was observed for H_2, CO production enhanced by the increase of AAEMs particles at the surface of the chars and more particularly potassium. In fact, Wigmans et al.[56] proposed that oxygen atoms can be trapped by potassium on the carbonaceous surface, which has been confirmed by Hashimoto et al.,[48] who suggested that K(O) was in a C−O−K form.

$$CH_4 + {\sim}O_{surf} \rightarrow CO + 2H_2 \quad (2)$$

$$CH_4 + 2{\sim}O_{surf} \rightarrow CO_2 + 2H_2 \quad (3)$$

Figure 7 presents the accumulated moles of H_2, CO, and CO_2 produced due to the heating and the methane cracking

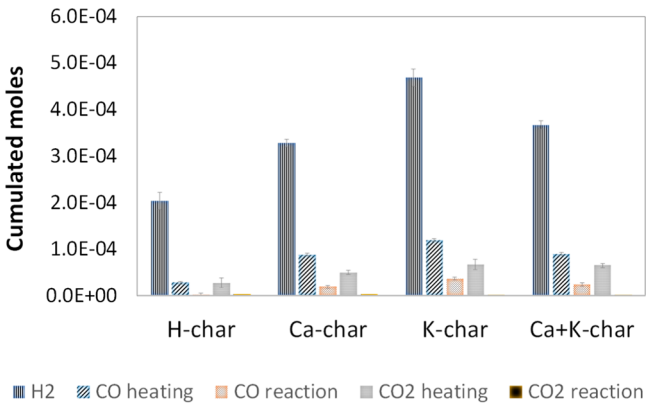

Figure 7. Cumulated moles of H_2, CO, and CO_2 produced during the catalytic methane cracking experiment at 700 °C for 2 h on a fixed bed of 20 mg of chars in an atmosphere of 10 vol % CH_4/90 vol % N_2 at a total flow rate of 80 mL/min (at 0 °C, 1 atm).

reaction. One can observe that hydrogen is the main product during the methane cracking reaction. Its production is increased by a factor of 1.6−2.3 using metal-loaded chars. Calculations have demonstrated that hydrogen is mostly produced by reaction 1 (more than 85%) whatever H-char or metal-loaded chars are used. As it has been previously discussed, higher productions of CO and CO_2 were also observed with metal-loaded chars, reaching values 5 times higher of CO and 2.2 higher of CO_2 for the K-char compared to the H-char. CO production was mainly due to the heating of the char and not to the methane cracking reaction. Calculations highlighted that CO was equally produced by the degassing and the methane cracking reaction for the H-char. However, the increase of the AAEMs at the surface of the metal-loaded chars tends to favor CO production during the degassing step since the ratio of CO produced due to degassing versus methane cracking reaction is of 1.1, 4.6, 3.3, and 3.7 for the H-char, Ca-char, K-char, and Ca+K-char, respectively.

Figure 8 presents the total (CO + H_2) production (normalized by the value obtained for the H-char) and the molar H_2/CO ratio. The total (CO + H_2) production is 1.9, 2.7, and 1.9 higher for the Ca-char, K-char, and Ca+K-char compared to the one of the H-char. Regarding the molar H_2/CO ratio, it is equal to 6.6 for the H-char taking into consideration the overall experiments. The ratio is decreased to 3.1, 3.0, and 3.2 using the Ca-char, K-char, and Ca+K-char. According to the syngas targeted application, it could be interesting to only recover the gas produced during the isothermal methane cracking to obtain a syngas rich in H_2. However, if CO is rather required, it should be interesting to only perform the heating step. The last option is to carry out the overall experiment and recover a syngas with a H_2/CO ratio comprised between 3 and 6 according to the char selected. This choice should be done regarding the specific biomass gasification unit and the end-use application selected for the syngas.

3.3. Correlation between Chars Surface Properties and Syngas Production. The increase of the syngas

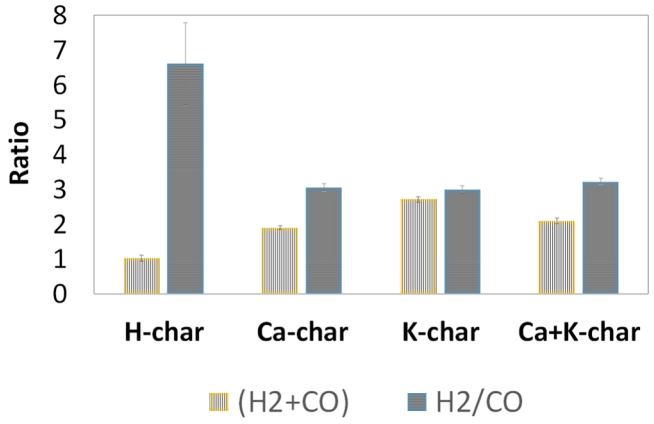

Figure 8. Comparison of the total moles of (H_2 + CO) and the molar H_2/CO ratio produced during the catalytic methane cracking experiment at 700 °C for 2 h on a fixed bed of 20 mg of chars in an atmosphere of 10 vol % CH_4/90 vol % N_2 at a total flow rate of 80 mL/min (at 0 °C, 1 atm). Values of the (H_2 + CO) moles were normalized according to the value for the H-char (for the sake of clarity).

production yield using the metal-loaded chars is correlated to their surface chemistry and physical properties. In fact, the AAEMs had a catalytic effect on both the oxygenated functions desorption during the outgassing step and on the isotherm catalytic methane cracking reaction at 700 °C. Potassium, such as depicted in the literature showed the best performances, increasing the initial syngas production by a factor 4. Ca-char and Ca+K-char showed similar activities increasing by a factor 2 the initial syngas production. Different reasons explain the better performances of the K-char. The reaction temperature was close to the potassium evaporation temperature, enhancing its mobility and reactivity. On the contrary, the higher content of silicon on the Ca-char and the interactions with the calcium particles were not favorable for the reactivity of the Ca-char. Synergetic effect of calcium and potassium on the reactivity, which has been described in the literature,[57] was not observed in this study. Even if the porosity and the specific surface area were decreased by the impregnation step, the AAEM-loaded chars exhibit higher reactivity than the H-char one, which confirms that both the chemical and physical properties of the chars are important for catalytic applications. Further research should investigate the possibilities to regenerate the metal-loaded char catalysts to increase their lifetime.[58]

4. CONCLUSIONS

Syngas production enhancement via catalytic methane cracking using metal-loaded chars, with a specific focus on the activity of two AAEMs, Ca and K, was investigated in this study. A meaningful increase of the syngas production (up to a factor 2.7) was observed in this work by modifying the surface properties of the char. The results are explained by the fact that AAEMs had a catalytic effect on both the oxygenated function desorption during the outgassing step and on the isotherm catalytic methane cracking reaction at 700 °C. Potassium, as depicted in the literature, showed the best performances. A catalytic methane cracking unit downstream from the biomass gasification reaction using metal-loaded char seems to be an interesting option to enhance syngas production with the possibility of H_2/CO ratio adjustment, which is a key economic parameter for syngas valorization.

AUTHOR INFORMATION

Corresponding Author

*E-mail: marion.ducousso@univ-pau.fr. Tel: +33 5 59 40 78 20.

ORCID

Marion Ducousso: 0000-0002-8197-2631

Notes

The authors declare no competing financial interest.

ACKNOWLEDGMENTS

The authors thank Christine Rolland for her expertise in the utilization of the

REFERENCES

(1) Liu, P.; Liu, W.-J.; Jiang, H.; Chen, J.-J.; Li, W.-W.; Yu, H.-Q. Modification of Bio-Char Derived from Fast Pyrolysis of Biomass and Its Application in Removal of Tetracycline from Aqueous Solution. *Bioresour. Technol.* **2012**, *121*, 235−240.

(2) Jindarom, C.; Meeyoo, V.; Kitiyanan, B.; Rirksomboon, T.; Rangsunvigit, P. Surface Characterization and Dye Adsorptive Capacities of Char Obtained from Pyrolysis/Gasification of Sewage Sludge. *Chem. Eng. J.* **2007**, *133* (1−3), 239−246.

(3) Ahmad, M.; Lee, S. S.; Rajapaksha, A. U.; Vithanage, M.; Zhang, M.; Cho, J. S.; Lee, S.-E.; Ok, Y. S. Trichloroethylene Adsorption by Pine Needle Biochars Produced at Various Pyrolysis Temperatures. *Bioresour. Technol.* **2013**, *143*, 615−622.

(4) Liu, W.-J.; Zeng, F.-X.; Jiang, H.; Zhang, X.-S. Preparation of High Adsorption Capacity Bio-Chars from Waste Biomass. *Bioresour. Technol.* **2011**, *102* (17), 8247−8252.

(5) Lee, Y.-W.; Park, J.-W.; Choung, J.-H.; Choi, D.-K. Adsorption Characteristics of SO_2 on Activated Carbon Prepared from Coconut Shell with Potassium Hydroxide Activation. *Environ. Sci. Technol.* **2002**, *36* (5), 1086−1092.

(6) Nielsen, S.; Minchin, T.; Kimber, S.; Van Zwieten, L.; Gilbert, J.; Munroe, P.; Joseph, S.; Thomas, T. Comparative Analysis of the Microbial Communities in Agricultural Soil Amended with Enhanced Biochars or Traditional Fertilisers. *Agric., Ecosyst. Environ.* **2014**, *191*, 73−82.

(7) Lehmann, J.; Rillig, M. C.; Thies, J.; Masiello, C. A.; Hockaday, W. C.; Crowley, D. Biochar Effects on Soil Biota − A Review. *Soil Biol. Biochem.* **2011**, *43* (9), 1812−1836.

(8) Hua, L.; Wu, W.; Liu, Y.; McBride, M. B.; Chen, Y. Reduction of Nitrogen Loss and Cu and Zn Mobility during Sludge Composting with Bamboo Charcoal Amendment. *Environ. Sci. Pollut. Res.* **2009**, *16* (1), 1−9.

(9) Seredych, M.; Hulicova-Jurcakova, D.; Lu, G. Q.; Bandosz, T. J. Surface Functional Groups of Carbons and the Effects of Their Chemical Character, Density and Accessibility to Ions on Electrochemical Performance. *Carbon* **2008**, *46* (11), 1475−1488.

(10) Dehkhoda, A. M.; Ellis, N. Biochar-Based Catalyst for Simultaneous Reactions of Esterification and Transesterification. *Catal. Today* **2013**, *207*, 86−92.

(11) Kastner, J. R.; Miller, J.; Geller, D. P.; Locklin, J.; Keith, L. H.; Johnson, T. Catalytic Esterification of Fatty Acids Using Solid Acid Catalysts Generated from Biochar and Activated Carbon. *Catal. Today* **2012**, *190* (1), 122−132.

(12) Klinghoffer, N. B.; Castaldi, M. J.; Nzihou, A. Catalyst Properties and Catalytic Performance of Char from Biomass Gasification. *Ind. Eng. Chem. Res.* **2012**, *51* (40), 13113−13122.

(13) Cha, J. S.; Park, S. H.; Jung, S.-C.; Ryu, C.; Jeon, J.-K.; Shin, M.-C.; Park, Y.-K. Production and Utilization of Biochar: A Review. *J. Ind. Eng. Chem.* **2016**, *40*, 1−15.

(14) Ravenni, G.; Sárossy, Z.; Ahrenfeldt, J.; Henriksen, U. B. Activity of Chars and Activated Carbons for Removal and Decomposition of Tar Model Compounds − A Review. *Renewable Sustainable Energy Rev.* **2018**, *94*, 1044−1056.

(15) Nanda, S.; Dalai, A. K.; Berruti, F.; Kozinski, J. A. K. Biochar as an Exceptional Bioresource for Energy, Agronomy, Carbon Sequestration, Activated Carbon and Specialty Materials. *Waste Biomass Valorization* **2016**, *7* (2), 201−235.

(16) Abu El-Rub, Z.; Bramer, E. A.; Brem, G. Experimental Comparison of Biomass Chars with Other Catalysts for Tar Reduction. *Fuel* **2008**, *87* (10−11), 2243−2252.

(17) Klinghoffer, N. Utilization of Char from Biomass Gasification in Catalytic Applications. *Ph.D. dissertation*, Columbia University, 2013.

(18) Shen, Y. Chars as Carbonaceous Adsorbents/Catalysts for Tar Elimination during Biomass Pyrolysis or Gasification. *Renewable Sustainable Energy Rev.* **2015**, *43*, 281−295.

(19) Saad, J. M.; Williams, P. T. Manipulating the H_2/CO Ratio from Dry Reforming of Simulated Mixed Waste Plastics by the Addition of Steam. *Fuel Process. Technol.* **2017**, *156*, 331−338.

(20) Cao, Y.; Gao, Z.; Jin, J.; Zhou, H.; Cohron, M.; Zhao, H.; Liu, H.; Pan, W. Synthesis Gas Production with an Adjustable H_2/CO Ratio through the Coal Gasification Process: Effects of Coal Ranks And Methane Addition. *Energy Fuels* **2008**, *22* (3), 1720−1730.

(21) De Caprariis, B.; Scarsella, M.; Petrullo, A.; De Filippis, P. Olive Oil Residue Gasification and Syngas Integrated Clean up System. *Fuel* **2015**, *158*, 705−710.

(22) Moliner, R.; Suelves, I.; Lazaro, M.; Moreno, O. Thermocatalytic Decomposition of Methane over Activated Carbons: Influence of Textural Properties and Surface Chemistry. *Int. J. Hydrogen Energy* **2005**, *30* (3), 293−300.

(23) Kim, M. Hydrogen Production by Catalytic Decomposition of Methane over Activated Carbons: Kinetic Study. *Int. J. Hydrogen Energy* **2004**, *29* (2), 187−193.

(24) Amin, A. M.; Croiset, E.; Epling, W. Review of Methane Catalytic Cracking for Hydrogen Production. *Int. J. Hydrogen Energy* **2011**, *36* (4), 2904−2935.

(25) Muradov, N.; Smith, F.; T-Raissi, A. Catalytic Activity of Carbons for Methane Decomposition Reaction. *Catal. Today* **2005**, *102−103*, 225−233.

(26) Fidalgo, B.; Menéndez, J. Á. Carbon Materials as Catalysts for Decomposition and CO_2 Reforming of Methane: A Review. *Chin. J. Catal.* **2011**, *32* (1−2), 207−216.

(27) Suelves, I.; Pinilla, J. L.; Lázaro, M. J.; Moliner, R. Carbonaceous Materials as Catalysts for Decomposition of Methane. *Chem. Eng. J.* **2008**, *140* (1−3), 432−438.

(28) Klinghoffer, N. B.; Castaldi, M. J.; Nzihou, A. Influence of Char Composition and Inorganics on Catalytic Activity of Char from Biomass Gasification. *Fuel* **2015**, *157*, 37−47.

(29) Feng, D.; Zhao, Y.; Zhang, Y.; Sun, S.; Meng, S.; Guo, Y.; Huang, Y. Effects of K and Ca on Reforming of Model Tar Compounds with Pyrolysis Biochars under H_2O or CO_2. *Chem. Eng. J.* **2016**, *306*, 422−432.

(30) Wigmans, T.; Haringa, H.; Moulijn, J. A. Nature, Activity and Stability of Active Sites during Alkali Metal Carbonate-Catalysed Gasification Reactions of Coal Char. *Fuel* **1983**, *62* (2), 185−189.

(31) McKee, D. W.; Spiro, C. L.; Kosky, P. G.; Lambi, E. J. *Catalytic Effect of Alkali Metal Salt in the Gasification of Coal Char*; General Electric Corporate Research & Development: Schenectady, NY, 1982.

(32) Mims, C. A.; Pabst, J. K. Role of Surface Salt Complexes in Alkali-Catalysed Carbon Gasification. *Fuel* **1983**, *62* (2), 176−179.

(33) Mims, C. A.; Pabst, J. K. Alkali-Catalyzed Carbon Gasification Kinetics: Unification of H_2O, D_2O, and CO_2 Reactivities. *J. Catal.* **1987**, *107* (1), 209−220.

(34) Dong, J.; Nzihou, A.; Chi, Y.; Weiss-Hortala, E.; Ni, M.; Lyczko, N.; Tang, Y.; Ducousso, M. Hydrogen-Rich Gas Production from Steam Gasification of Bio-Char in the Presence of CaO. *Waste Biomass Valorization* **2017**, *8* (8), 2735−2746.

(35) Wigmans, T.; Tromp, P.; Moulijn, J. A. On the Interpretation of Reactivity Measurements during Potassium Catalysed Carbon Gasification Reactions. *Carbon* **1984**, *22* (3), 319−321.

(36) Mims, C. A.; Chludzinski, J. J., Jr; Pabst, J. K.; Baker, R. T. K. Potassium-Catalyzed Gasification of Graphite in Oxygen and Steam. *J. Catal.* **1984**, *88* (1), 97−106.

(37) Yokoyama, S.; Miyahara, K.; Tanaka, K.; Takakuwa, I.; Tashiro, J. Catalytic Reduction of Carbon Dioxide. 1. Reduction of Carbon Dioxide with Carbon Carrying Potassium Carbonate. *Fuel* **1979**, *58* (7), 510−514.
(38) Vamvuka, D.; Karouki, E.; Sfakiotakis, S.; Salatino, P. Gasification of Waste Biomass Chars by Carbon Dioxide via Thermogravimetry—Effect of Catalysts. *Combust. Sci. Technol.* **2012**, *184* (1), 64−77.
(39) Kuzhiyil, N.; Dalluge, D.; Bai, X.; Kim, K. H.; Brown, R. C. Pyrolytic Sugars from Cellulosic Biomass. *ChemSusChem* **2012**, *5* (11), 2228−2236.
(40) ISO: Organisation Internationale de Normalisation. *Biocombustible Solides : Méthode de La Détermination de Teneur En Cendres*. ISO 18122:2015.2015.
(41) Nzihou, A.; Stanmore, B.; Sharrock, P. A Review of Catalysts for the Gasification of Biomass Char, with Some Reference to Coal. *Energy* **2013**, *58*, 305−317.
(42) Cao, X.; Ma, L.; Gao, B.; Harris, W. Dairy-Manure Derived Biochar Effectively Sorbs Lead and Atrazine. *Environ. Sci. Technol.* **2009**, *43* (9), 3285−3291.
(43) Li, H.; Dong, X.; Da Silva, E. B.; De Oliveira, L. M.; Chen, Y.; Ma, L. Q. Mechanisms of Metal Sorption by Biochars: Biochar Characteristics and Modifications. *Chemosphere* **2017**, *178*, 466−478.
(44) Shinogi, Y. Nutrient Leaching from Carbon Products of Sludge. ASAE/CSAE Annual International Meeting 2004. American Society of Agricultural and Biological Engineers, St. Joseph, MO, 2004; Paper number 0440063.
(45) Duan, Y.; Luebke, D. R.; Pennline, H. W.; Li, B.; Janik, M. J.; Halley, J. W. Ab Initio Thermodynamic Study of the CO_2 Capture Properties of Potassium Carbonate Sesquihydrate, $K_2CO_3{\cdot}1.5H_2O$. *J. Phys. Chem. C* **2012**, *116* (27), 14461−14470.
(46) Ducousso, M.; Weiss-Hortala, E.; Nzihou, A.; Castaldi, M. J. Reactivity Enhancement of Gasification Biochars for Catalytic Applications. *Fuel* **2015**, *159*, 491−499.
(47) Winbo, C.; Rosen, E.; Heim, M. Thermal Analytical Study of the Decomposition of $K_2Ca_2(CO_3)_3$. *Acta Chem. Scand.* **1998**, *52*, 431−434.
(48) Hashimoto, K.; Miura, K.; Xu, J.-J.; Watanabe, A.; Masukami, H. Relation between the Gasification Rate of Carbons Supporting Alkali Metal Salts and the Amount of Oxygen Trapped by the Metal. *Fuel* **1986**, *65* (4), 489−494.
(49) Wang, J.; Jiang, M.; Yao, Y.; Zhang, Y.; Cao, J. Steam Gasification of Coal Char Catalyzed by K_2CO_3 for Enhanced Production of Hydrogen without Formation of Methane. *Fuel* **2009**, *88* (9), 1572−1579.
(50) Ganga Devi, T.; Kannan, M.P. Calcium Catalysis in Air Gasification of Cellulosic Chars. *Fuel* **1998**, *77* (15), 1825−1830.
(51) McKee, D. W. Mechanisms of the Alkali Metal Catalysed Gasification of Carbon. *Fuel* **1983**, *62* (2), 170−175.
(52) Hüttinger, K. J.; Minges, R. Influence of the Catalyst Precursor Anion in Catalysis of Water Vapour Gasification of Carbon by Potassium: 1. Activation of the Catalyst Precursors. *Fuel* **1986**, *65* (8), 1112−1121.
(53) Amin, A. M.; Croiset, E.; Epling, W. Review of Methane Catalytic Cracking for Hydrogen Production. *Int. J. Hydrogen Energy* **2011**, *36* (4), 2904−2935.
(54) Abbas, H. F.; Daud, W. M. A. W. Deactivation of Palm Shell-Based Activated Carbon Catalyst Used for Hydrogen Production by Thermocatalytic Decomposition of Methane. *Int. J. Hydrogen Energy* **2009**, *34* (15), 6231−6241.
(55) Suelves, I.; Lázaro, M. J.; Moliner, R.; Pinilla, J. L.; Cubero, H. Hydrogen Production by Methane Decarbonization: Carbonaceous Catalysts. *Int. J. Hydrogen Energy* **2007**, *32* (15), 3320−3326.
(56) Wigmans, T.; Elfring, R.; Moulijn, J. A. On the Mechanism of the Potassium Carbonate Catalysed Gasification of Activated Carbon: The Influence of the Catalyst Concentration on the Reactivity and Selectivity at Low Steam Pressures. *Carbon* **1983**, *21* (1), 1−12.
(57) Wang, J.; Yao, Y.; Cao, J.; Jiang, M. Enhanced Catalysis of K_2CO_3 for Steam Gasification of Coal Char by Using $Ca(OH)_2$ in Char Preparation. *Fuel* **2010**, *89* (2), 310−317.
(58) Dufour, A.; Celzard, A.; Fierro, V.; Broust, F.; Courson, C.; Zoulalian, A.; Rouzaud, J. N. Catalytic Conversion of Methane over a Biomass Char for Hydrogen Production: Deactivation and Regeneration by Steam Gasification. *Appl. Catal., A* **2015**, *490*, 170−180.